Longitudinal In Vivo Characterization of the Streptozotocin-Induced Diabetic Mouse Model: Focus on Early Inner Retinal Responses

Jurgen Sergeys,[1] Isabelle Etienne,[2] Inge Van Hove,[1,2] Evy Lefevere,[1] Ingeborg Stalmans,[3] Jean H. M. Feyen,[2] Lieve Moons,[1] and Tine Van Bergen[2]

[1]Neural Circuit Development and Regeneration Research Group, Department of Biology, Zoological Institute, KU Leuven, Leuven, Belgium
[2]Oxurion NV, Leuven, Belgium
[3]Laboratory of Experimental Ophthalmology, Department of Neurosciences, O&N II, KU Leuven, Leuven, Belgium

PURPOSE. The goal of this study was to perform an extensive temporal characterization of the early pathologic processes in the streptozotocin (STZ)–induced diabetic retinopathy (DR) mouse model, beyond the vascular phenotype, and to investigate the potential of clinically relevant compounds in attenuating these processes.

METHODS. Visual acuity and contrast sensitivity (CS) were studied in the mouse STZ model until 24 weeks postdiabetes onset. ERG, spectral domain optical coherence tomography (SD-OCT), leukostasis, and immunohistochemistry were applied to investigate neurodegeneration, inflammation, and gliosis during early-, mid- and late-phase diabetes. Aflibercept or triamcinolone acetonide (TAAC) was administered to investigate their efficacy on the aforementioned processes.

RESULTS. Visual acuity and CS loss started at 4 and 18 weeks postdiabetes onset, respectively, and progressively declined over time. ERG amplitudes were diminished and OP latencies increased after 6 weeks, whereas SD-OCT revealed retinal thinning from 4 weeks postdiabetes. Immunohistochemical analyses linked these findings to retinal ganglion and cholinergic amacrine cell loss at 4 and 8 weeks postdiabetes onset, respectively, which was further decreased after aflibercept administration. The number of adherent leukocytes was augmented after 2 weeks, whereas increased micro- and macroglia reactivity was present from 4 weeks postdiabetes. Aflibercept or TAAC showed improved efficacy on inflammation and gliosis.

CONCLUSIONS. STZ-induced diabetic mice developed early pathologic DR hallmarks, from which inflammation seemed the initial trigger, leading to further development of functional and morphologic retinal changes. These findings indicate that the mouse STZ model is suitable to study novel integrative non-vascular therapies to treat early DR.

Keywords: diabetic retinopathy, streptozotocin (STZ)-induced mouse model, visual acuity, electroretinography, neurodegeneration, inflammation, gliosis

Due to the Western lifestyle, increased life expectancy at birth, and societal aging, prevalence of diabetes mellitus (DM) type I and II is expected to rise from 415 million in 2015 to 640 million in 2040.[1,2] Diabetic retinopathy (DR) is the most common microvascular complication of DM and a chronic and progressive eye disease causing irreversible vision loss and blindness in the working-age population in developed countries.[3–5] Furthermore, global studies describe that one out of three diabetes patients will develop DR, highlighting the enormous socioeconomic impact of the disease.[5,6]

DR is clinically characterized by vascular abnormalities such as microaneurysms, hemorrhages, capillary occlusion, diabetic macular edema (DME), and neovascularization in the posterior part of the eye. Both diagnosis and treatment are currently focused on the vascular pathology, and they only target advanced stages of the disease when vision has already been significantly affected.[4,7–11] However, it becomes increasingly clear that DR is not solely a microvascular complication, but that neurodegeneration,[10,12] and inflammation[13,14] are also important processes affecting disease onset and progression, possibly in a stage prior to the vasculopathy. Although there is still much controversy in literature regarding the time course of neurodegeneration in DR,[15] it is now generally recognized that diabetes affects the neural retina, as observed by retinal dysfunction and vision loss both in humans suffering from DR and in animal models.[16–18] Additional evidence, mostly from clinical studies, indicates that DR is a chronic low-grade inflammatory disease, since it has been shown that pro-inflammatory growth factors, cyto- and chemokines (e.g., TNF-α, IL-1β, IFN-γ, etc.) are upregulated in serum, aqueous, or vitreous humor samples of diabetic patients.[19] These inflammatory mediators will not only attract leukocytes to the vascular endothelium, but will also reactivate microglia during DR, resulting in their uncontrolled proliferation, provoking

retinal toxicity, and neuronal cell death.[20] Finally, macroglial cells that normally maintain retinal homeostasis and support the neuronal tissue, are also identified as important players during DR development and recent studies suggest that glial reactivity (gliosis) in the retina is coupled to early neuronal impairment.[21-23]

Thus, while neurodegeneration, inflammation, and gliosis are increasingly acknowledged as important processes, besides vascular changes, during early DR development, the specific time course of these pathologic hallmarks remains to be elucidated. The most common preclinical diabetic animal model described in literature is the streptozotocin (STZ)-induced diabetic mouse model.[24] While there is still controversy in literature related to the occurrence of vascular changes in this model,[25,26] a limited number of studies already nicely described nonvascular changes, such as functional[16,27,28] and morphologic changes,[29,30] as well as alterations in early DR hallmarks, including leukostasis and correlated increased cytokine levels.[14,31-34] Since a detailed and time-related determination of the cellular processes in the STZ-induced DR mouse model is lacking, the aim of this study was to perform an extensive temporal characterization of the pathologic processes, beyond the vascular phenotype. First, we used functional and morphologic noninvasive techniques that allow longitudinal investigations, such as OptoMotry, ERG, and spectral domain optical coherence tomography (SD-OCT). Secondly, more in-depth, cell-specific information via postmortem analysis of retinal neurodegeneration, inflammation, and gliosis at multiple time points after diabetes onset was retrieved using immunohistochemical analysis. Since VEGF inhibition and steroids are currently the standard of care therapy for DR, the efficacy of these compounds on the various pathologic hallmarks of DR was also studied to provide proof of concept that the diabetic STZ mouse model can be used for the evaluation of new therapeutic strategies to halt DR progression.

METHODS

Animals

All experimental animal procedures were performed according the standards in the ARVO Statement for the Use of Animals in Ophthalmic and Vision Research and the EC Directive 89/609/EEC for animal experiments. All experiments were also approved by the Institutional Animal Care and Research Advisory Committee of KU Leuven (P110/2015 and P203/2015), and according to the European Directive 2010/63/EU.

STZ-Induced Diabetes Mice Model

In order to investigate the different processes involved in the pathology of DR, the STZ-induced diabetes mouse (*Mus musculus*) model was used, since this is the most common diabetic mouse model described in literature.[24] In detail, male C57BL/6J mice (3–5 weeks old) were rendered diabetic via 5 consecutive daily intraperitoneal (IP) STZ (50 mg/kg) injections, freshly dissolved in Na-citrate buffer (pH 4.5). Control (nondiabetic) mice received only buffer injections. Development of diabetes was weekly monitored via blood glucose levels (OneTouch Verio; LifeScan, Beerse, Belgium). Only animals with consistent elevated blood glucose levels (>250 mg/dL) were considered diabetic and used in the study. Mice were euthanized for leukostasis and postmortem analysis during early- (2–6 weeks), mid- (8–12 weeks) and late-phase diabetes (20–24 weeks after diabetes onset).

Intravitreal Administration of Compounds

A subset of mice was intravitreally (IVT) injected with compounds that are currently used in clinical practice for the treatment of DR, aflibercept (Eylea; Bayer, Leverkusen, Germany) and triamcinolone acetonide (TAAC, Kenacort; Bristol-Myers Squibb, New York, NY, USA).[35,36] Mice were deeply anesthetized via inhalatory isoflurane (4% Iso-Vet; Dechra, Northwich, UK) and the eyes were further locally anesthetized with oxybuprocaine (0.4% Unicaine; Thea Pharma, Wetteren, Belgium) eye drops. IVT injections (1 μL) were performed with a small glass capillary (50–70 μm diameter), connected to a microinjector (Micro4, microsyringe pump controller; World Precision Instruments, Sarasota, FL, USA). A group of mice was injected with aflibercept (40 μg/eye), a recombinant fusion protein inhibiting both VEGF and placental growth factor (PlGF), and its effect was evaluated by using optomotor, leukostasis, and immunohistochemical readouts. Another group of mice was treated with TAAC (40 μg/eye) for evaluating its effect on retinal inflammation. Respective buffer solutions were used as negative vehicle controls. The control buffer for aflibercept was 10 mM NaH_2PO_4, 40 mM NaCl, 5% sucrose, 0.03% Tween 20 at pH 6.2. The vehicle for TAAC consisted out of NaCl for isotonicity, 0.5% (wt/vol) carboxymethylcellulose sodium, 0.015% (wt/vol) and polysorbate 80 in H_2O at pH 6 to 7.5. As long-term weekly IVT injections would have led to anesthesia-related body weight loss, treatment was only initiated 1 week before being euthanized (i.e., in week 7 postdiabetes onset). Injections were given every other day, with a total of four injections, based on the short half-life of the compounds in rodent eyes (data not shown). The day after the last injection, animals were euthanized (i.e., at 8 weeks after diabetes onset).

Optokinetic Tracking Response

Mice were biweekly (from 0–24 weeks after diabetes onset) subjected to a virtual-reality chamber, used to test visual behavior, via the optokinetic tracking response (OKT; OptoMotry, Cerebral Mechanics, Alberta, Canada), as described by Prusky et al.[37] At 8 weeks after diabetes onset, visual acuity of diabetic mice treated with aflibercept or buffer was also investigated (Fig. 1). Briefly, an unrestrained mouse was placed on a platform in the center of an arena, which exists out of four computer screens. Vertical sine-wave gratings (black-white), represented as a vertical cylinder, were projected on the screens and moved at 12°/second around the mouse. A video camera was placed on top of the arena to provide real-time video data. Special frequency (SF) thresholds were measured for each eye under 100% contrast, via a simple staircase procedure were different SF varied randomly. Contrast sensitivity (CS) was assessed on different SF (0.103, 0.192 and 0.272, inverse Michelson contrast), while contrast varied randomly via staircase procedure.

Electroretinography

To assess retinal functionality via full-field ERG, overnight dark-adapted mice (4, 6, 8, 12, and 20 weeks postdiabetes onset) were stimulated by UTAS Ganzfeld light source (UTAS BigShot E-3000; LKC Technologies, Inc., Gaithersburg, MD, USA) in order to stimulate both eyes simultaneously.[38] Diabetic mice were compared to nondiabetic animals, with 5 to 6 mice per condition. Mice were anesthetized by an IP injection of 75 mg/kg body weight ketamine (Anesketin; Eurovet, Bladel, The Netherlands) combined with 1 mg/kg medetomidine (Domitor; Pfizer, New York, NY, USA) and pupils were dilated with 0.5% tropicamide (Tropicol; Thea Pharma, Wetteren, Belgium) and
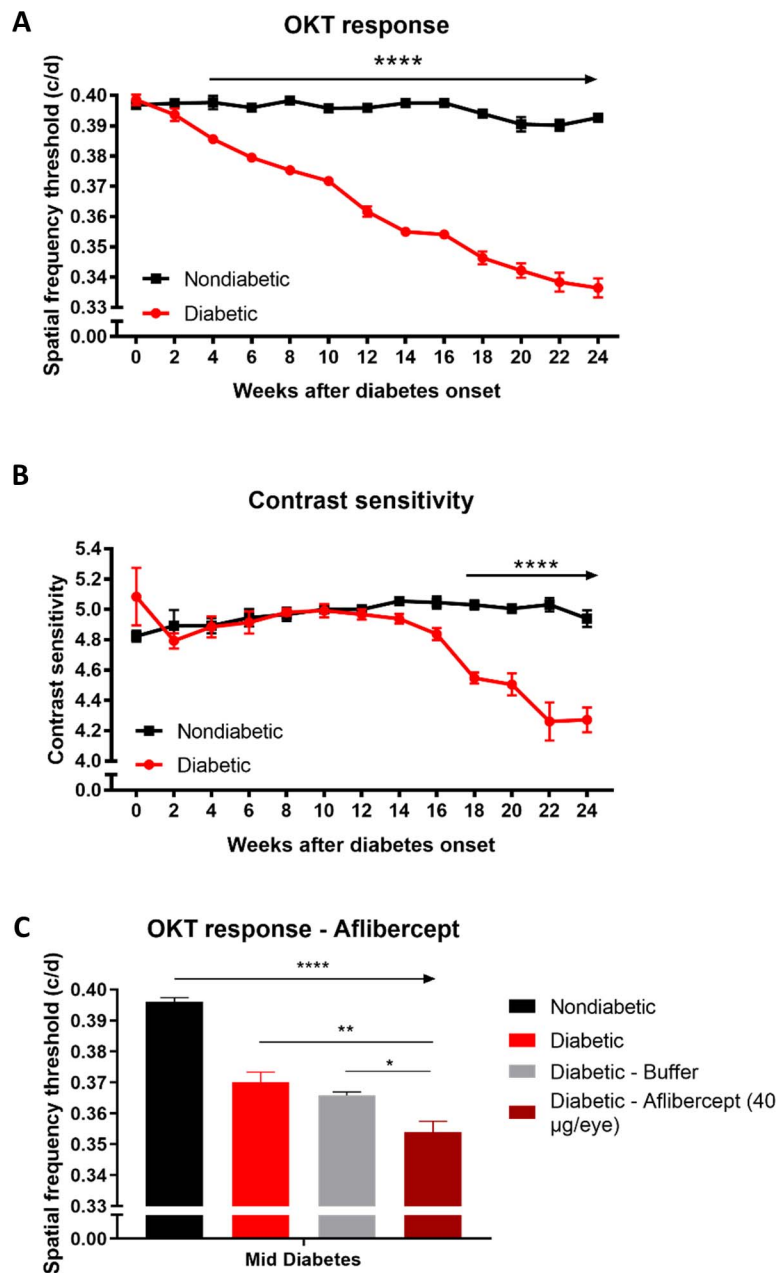
FIGURE 1. Progressive decline of OKT response and CS. (**A**) Visual acuity of nondiabetic mice did not change over time from 0 until 24 weeks, while diabetic mice showed progressive loss of visual function. Visual acuity was reduced with 4% at 4 weeks and 14% at 24 weeks postdiabetes onset. (**B**) Measurement of CS, at a spatial frequency of 0.272 cyc/deg, revealed a progressive decrease in diabetic animals from 10% at 18 weeks postdiabetes onset, that reached a maximum reduction of 14% at 24 weeks after diabetic onset. (**C**) IVT treatment of aflibercept (40 μg/eye) was performed every other day at week 7, with a total of 4 injections. Eight weeks post-diabetes onset, SF thresholds for all diabetic animals were still reduced compared to control animals, but aflibercept-injected mice developed a significant additional loss of 3%, compared to buffer-injected mice. Data are shown as mean ± SEM, $n = 5$-7. $*P < 0.05$. $**P < 0.01$. $****P < 0.0001$.

15% phenylephrine (Thea Pharma). A ground electrode was placed in the tail base, the reference electrode in the left cheek and contact lenses with gold wire served as signal electrodes. Eyes were kept moist with saline, which was also used as a conductor for the electrical signal. A nine-step stimulation protocol with increasing flash luminance was applied ranging from -3.10 to 1.40 log cd.s/m^2. The results of the lower light intensities (-3.10 to -0.60 log cd.s/m^2) were averaged from three light flashes, interspaced with 10 seconds. For the next two flash stimuli (-0.10 and 0.40 log cd.s/m^2), two flashes with 30 seconds intermediate time were averaged. Step 8 and 9

(highest light intensities, 0.90 and 1.40 log cd.s/m^2) were averaged over two flashes separated with 45 seconds. Oscillatory potentials (OPs) were automatically filtered out by the ERG software. The latencies and amplitudes of OP1-3 were measured separately. Averaged runs were used to measure a-, b-wave and OP amplitudes as well as latency and implicit times. According to the current convention, the a-wave amplitude was determined at a specific time point (8 ms after light flash) preceding the a-wave trough, while b-wave amplitude was measured from the trough of the a-wave to the maximal amplitude following the OPs. Latency was determined

from flash onset to the a-wave trough and b-wave implicit time from flash onset to b-wave maximal amplitude, all according to previous literature describing ERG measurements.[39] Final data was retrieved from averaging left and right eye.[40] Electroretinograms (Figs. 2, 3) were adjusted to start at the zero point, in order to fit the overlays more appropriately. After imaging, an IP injection of atipamezole (1 mg/kg, Antisedan; Pfizer, New York, NY, USA) was administered to reverse anesthesia and eye ointment (Vidisic; Bausch + Lomb, Rochester, NY, USA) was used to prevent dry eyes.

Optical Coherence Tomography

A SD-OCT system (Envisu R2210; Bioptigen, Morrisville, NC, USA) was applied for thickness measurements of the retinal layers at week 4, 8, and 24 after diabetes onset. Animals were anesthetized via ketamine and medetomidine as described previously. When sedated, tropicamide eye drops were administered for pupil dilatation. Next, SD-OCT was performed using 100 consecutive B-scan lines composed of 1000 A-scans, in a 1.4×1.4 mm plane. Anesthesia was reversed with atipamezole and eye ointment (Bausch + Lomb) was applied to prevent dry eyes. Total retinal thickness and thickness of separate retinal layers was analyzed using commercial software (InVivoVue Diver 2.2; Bioptigen). A fixed 5×5 grid, highlighting 25 points that can be measured on the retina, was centered on the optic disc. Using those points, at minimum 10 measurements were performed and averaged (Fig. 4A). Separate layers were analyzed as shown in Figure 4B, by placing cursors (orange asterisks) on each boundary of two different retinal layers. Based on these cursors, the software (Bioptigen) automatically calculated the thickness of the different retinal layers. Since retinal morphologic changes during DR are mostly described in patients in the inner retinal layers,[41,42] separate layer analysis was limited to thickness measurements of the ganglion cell complex (GCC, including nerve fiber layer [NFL], ganglion cell layer [GCL], and inner plexiform layer [IPL]), as well as measurements of the NFL-GCL complex.

Vessel Leakage Assays

In-life fluorescein angiography (FA) was biweekly performed with a confocal scanning laser ophthalmoscope (HRA, Heidelberg Spectralis; Heidelberg Engineering, Heidelberg, Germany), to longitudinally study vascular leakage from 0 to 24 weeks postdiabetes onset. A 50° angle lens and excitation light with a wavelength of 488 nm were used for retinal blood vessels imaging. Before imaging, pupils of anesthetized animals were dilated by tropicamide, and a fundus picture of the right eye was obtained before fluorescein injection. After IP injection of 200 µL of 2% (wt/vol) sodium-fluorescein, FA scans were collected at 3 and 15 minutes after fluorescein injection, representing early and late leakage phase, as described by Chung et al.[43] At the end of the procedure, anesthesia was reversed with atipamezole and eyes were covered with eye ointment (Bausch + Lomb).

Vessel leakage was also analyzed using FITC-BSA and TRITC-dextran retro-orbital injections. Mice were anesthetized with isoflurane 4% and retro-orbitally injected, during early (week 4) and midterm diabetes (week 8) with FITC-albumin (20 mg/mL, Sigma-Aldrich Corp., Overijse, Belgium) for visualizing the leakage and TRITC-dextran (2000 kDa, 10 mg/mL, Thermo Fisher Scientific, Inc., Asse, Belgium) for visualizing the blood vessels. The dyes circulated for 30 minutes in awake animals, after which mice were euthanized and eyes were enucleated and fixated overnight in 1% paraformaldehyde (PFA) in PBS. The next day, retinal whole mounts were dissected and

mounted on glass slides with mowiol (Sigma-Aldrich Corp.). Images were taken with ×20 objective with an upright microscope (LEICA DM6 B; Leica, Wetzlar, Germany).

Finally, vitreous leakage was studied with a fluorophotometer (i.e., the mouse Fluorotron Master; OcuMetrics, Inc., Mountain View, CA, USA). Mice (8 and 20 weeks after diabetes onset) were subcutaneously injected with 200 µL of 2.5% fluorescein, which circulated for 40 minutes in awake animals. Mice were anesthetized with the above mentioned ketamine/medetomidine mixture and tropicamide was applied on both eyes to assure dilation. A scan of both eyes was taken and the anesthesia was reversed with atipamezole. The fluorescein concentration (ng/mL) of both eyes was analyzed in the middle of the vitreous peak and averaged to obtain quantitative vitreous leakage levels.

Leukostasis

Retinal leukostasis (i.e., increased leukocyte adhesion to the capillary endothelium in the retina), was investigated in early (2–4 weeks), mid- (8 weeks), and late-stage (20 weeks) diabetic mice. Leukostasis of diabetic mice treated with TAAC or buffer was also analyzed at 8 weeks postdiabetes onset. The animals were anesthetized using an IP injection of 30 mg/kg sodium pentobarbital (Nembutal, Ceva, Brussels, Belgium), and transcardially perfused. First erythrocytes and nonadherent leukocytes were washed out with NaCl 0.9% and heparin (71 mg/L) for 5 minutes, using a perfusion rate of 2 to 3 mL/minute. Next, adherent leukocytes were labelled with FITC-concanavalin A lectin (FITC-ConA, 40 µg/mL, Vector Laboratories, Burlingame, CA, USA), via perfusion of 25 mL in 2 to 3 minutes. The last step included removal of the unbound FITC-ConA by flushing again heparinized NaCl 0.9% through the blood vessels. Mice were euthanized, eyes were enucleated, overnight incubated in 1% PFA and retinas were flatmounted. Visualization and live counting of the total number of stained adherent leukocytes in the arterioles and venules was performed by a blinded investigator, using a microscope (Leica DM IL LED; Leica). High quality representative pictures were taken on a confocal microscope (Olympus FV1000; Olympus Corp., Tokyo, Japan).[44]

Immunohistochemistry and Histologic Analysis

General. Embedded paraffin eyes collected at representative early (4 weeks), mid- (8 weeks), and late (24 weeks after diabetes onset) time points, including aflibercept, TAAC and buffer-treated eyes, were used for all the (immuno)histological stainings. Eyes were serially sectioned in 7-µm thick sagittal slices. On every first slide of each series (5 slides/series), a hematoxylin and eosin (H&E) staining was performed to determine the general retinal morphology and the optic nerve head, since analysis was performed on three sections adjacent to both sides of the optic nerve. Before administration of the primary antibody (Ab), sections were deparaffinized, antigens were retrieved using PT module (Thermo Fisher Scientific, Inc.) with modified citrate buffer (Agilent; S1699) and endogenous peroxidases were blocked by immersing the slides in methanol (VWR, Leuven, Belgium) containing 0.3% hydrogen peroxide (VWR) for 20 minutes.

Neurodegeneration. Retinal neuronal cell death was studied using antibodies against RNA-binding protein with multiple splicing (RBPMS) and choline-acetyl-transferase (ChAT) to label retinal ganglion cells (RGCs) and cholinergic amacrine cells, respectively. Sections were incubated overnight with primary Abs for RBPMS (1/200; 1830-RBPMS, Phospho-Solutions)[45] or ChAT (1/200; AB144P, Chemicon).[46] The second day, secondary Abs were added for 45 minutes (i.e.,
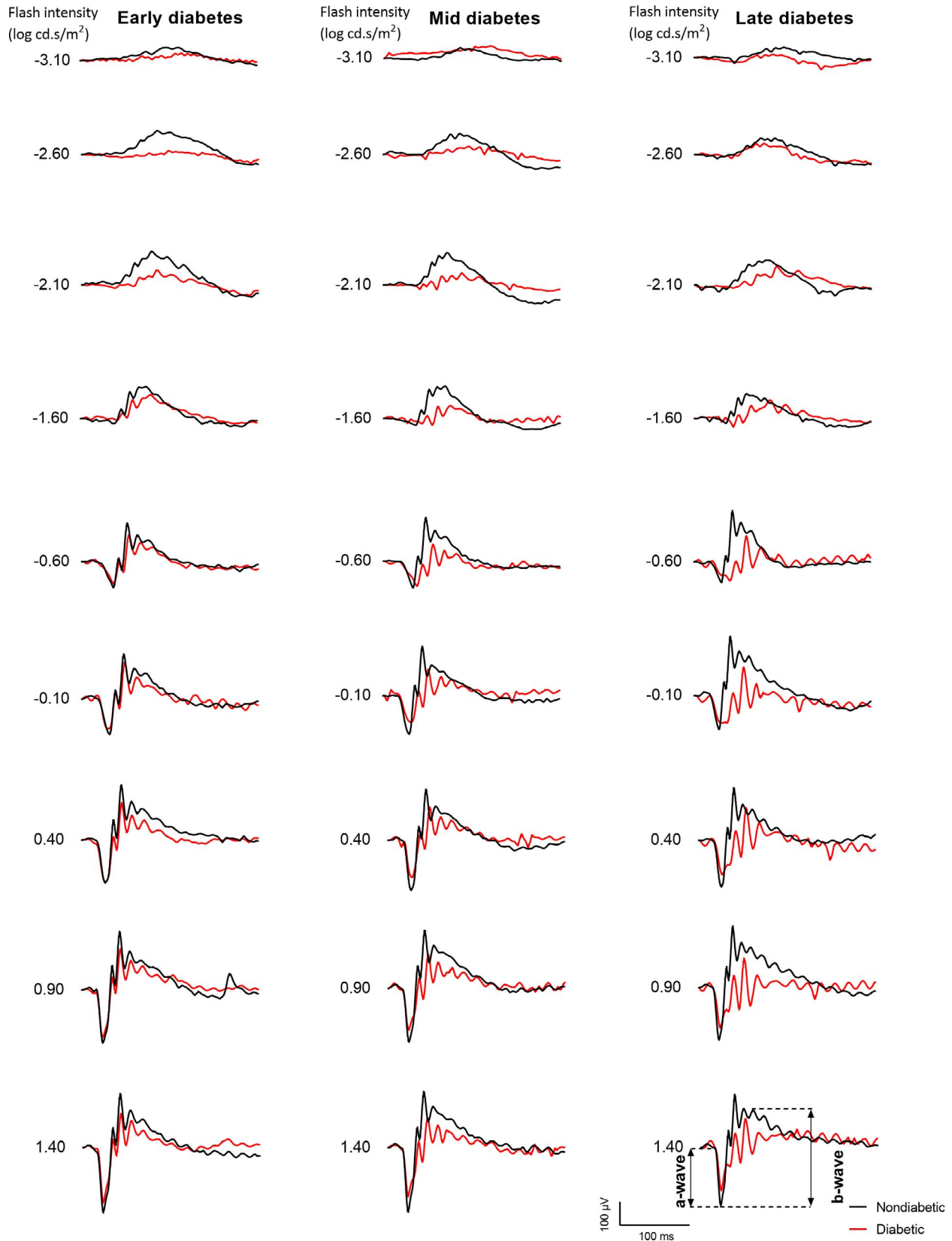
FIGURE 2. Diabetes-induced progressive decline of a- and b-wave amplitudes and increase of latency and implicit times. ERG measurements were performed at 6 (early), 12 (mid-), and 20 weeks (late) after diabetes onset. Representative electroretinograms are shown for nondiabetic (*black*) and diabetic (*red*) animals. Measurements were performed as described in Kinoshita & Peachey.[39] Amplitudes of a- and b-wave declined early after development of diabetes in the STZ-treated mice compared to control mice, while the latency and implicit times increased over time. *N* = 5 to 6 animals per group. *Double-headed arrows* reaching toward the dashed lines represent a- and b-wave.
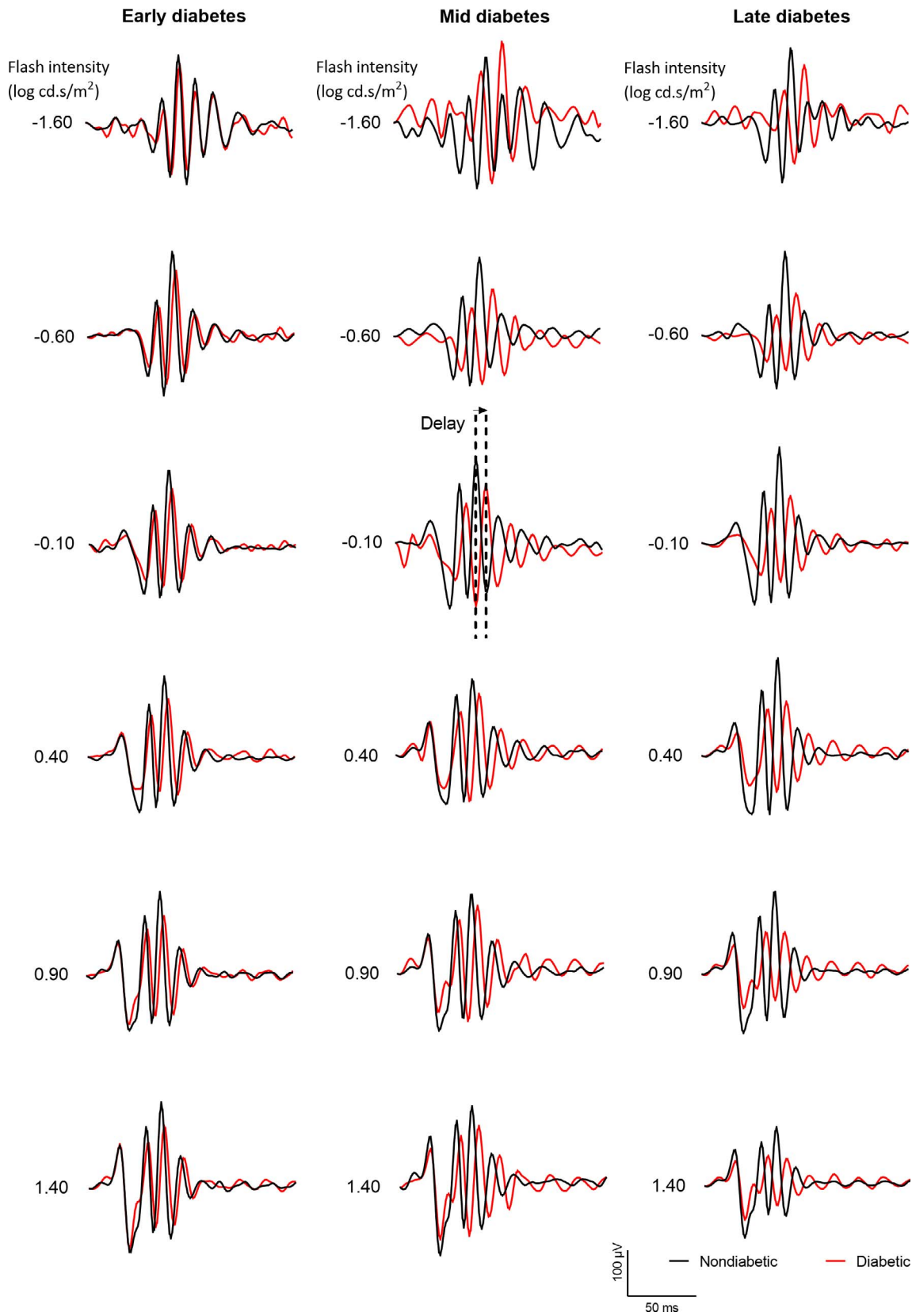
FIGURE 3. Diabetes-induced progressive increase of OP latency. Representative OPs of early- (6 weeks), mid- (12 weeks) and late- (20 weeks) term diabetes are shown for nondiabetic (*black*) and diabetic (*red*) animals. OP latency of diabetic animals was significantly increased from 6 weeks postdiabetes onset on and became more pronounced at prolonged diabetic states. $N = 5$ to 6 animals per group. *Arrow* between the *dashed lines* represent the latency delay between diabetic and nondiabetic mice.
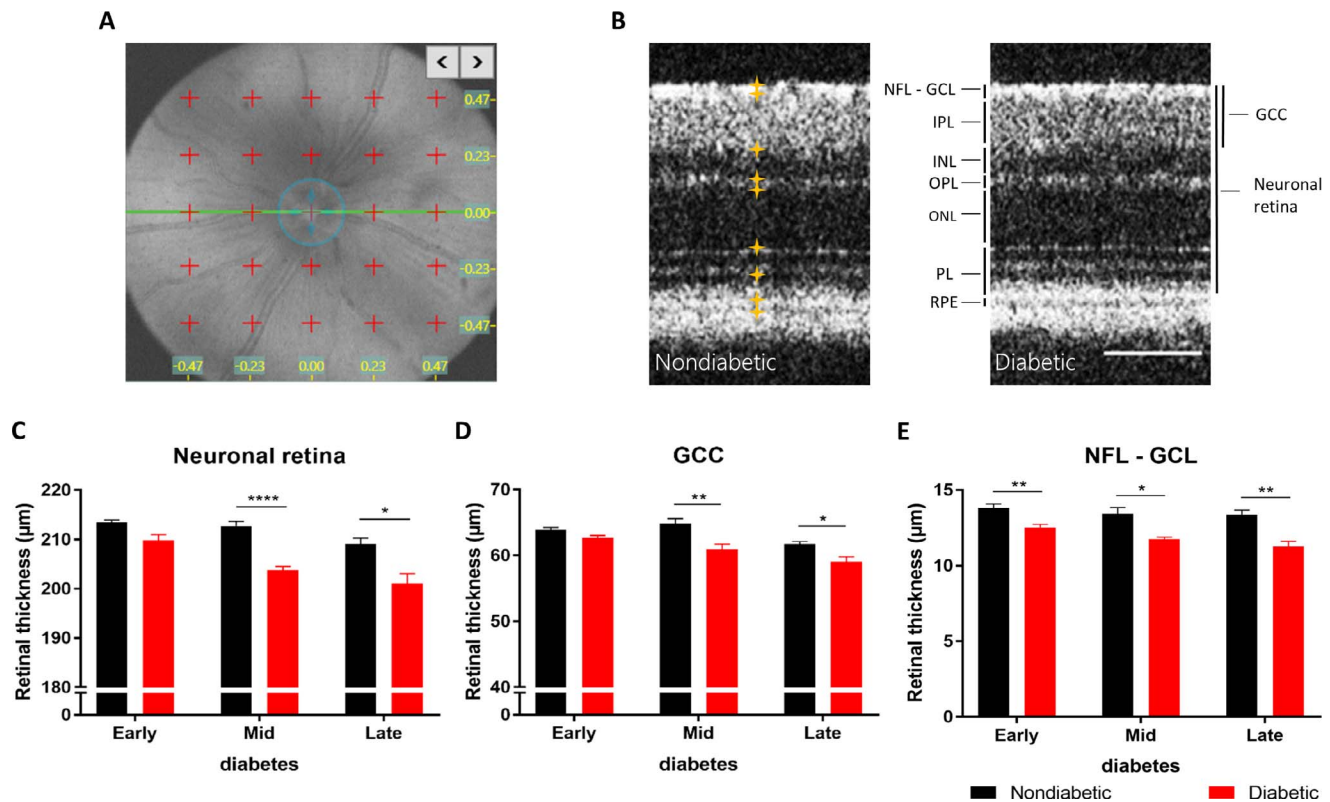
FIGURE 4. Retinal thickness measurements during early-, mid-, and late-diabetes. SD-OCT was applied to mice suffering from early- (4 weeks), mid- (8 weeks), and late-stage (24 weeks) diabetes. (A) A fixed 5 × 5 grid was placed over the fundus to indicate points (*red asterisks*) for thickness measurements. (B) Representative OCT images of mice suffering from diabetes for 8 weeks and age-matched nondiabetic controls. *Orange asterisks* indicate the manually placed cursors at each border of different retinal layers. (C) During mid- and late diabetes, the neuronal retina thickness was decreased with 4% (212.7 ± 0.9 μm [control] vs. 203.8 ± 0.7 μm [diabetic] and 209 ± 1.1 μm [control] vs. 201.0 ± 2.0 μm [diabetic], respectively). Part of this neuronal thinning, progresses from (D) GCC thinning (6%, 64.9 ± 0.7 μm [control] vs. 60.9 ± 0.8 μm [diabetic]) during midterm diabetes and 4% during late-phase diabetes (61.8 ± 0.4 μm [control] vs. 59.1 ± 0.7 μm [diabetic]) and (E) GCL-NFL thinning during early (9% reduction, 13.8 ± 0.3 μm [control] vs. 12.5 ± 0.2 μm [diabetic]), mid- (12% reduction, 13.4 ± 0.4 μm [control] vs. 11.8 ± 0.1 μm [diabetic]), and late diabetes (16% reduction, 13.4 ± 0.3 μm [control] vs. 11.3 ± 0.3 μm [diabetic]). Data are shown as mean + SEM, $n = 4$ to 13. *Scale bar*: 100 μm. *$P < 0.05$. **$P < 0.01$. ****$P < 0.0001$. NFL, nerve fiber layer; GCL, ganglion cell layer; IPL, inner plexiform layer; GCC, ganglion cell complex; INL, inner nuclear layer; OPL, outer plexiform layer; ONL, outer nuclear layer; PL, photoreceptor layer.

goat anti-rabbit-biotinylated; 1/300, 111-065-144, rabbit anti-goat-HRP; 1/100, 305-035-003, Jackson, West Grove, PA, USA). The Ab-complexes were visualized using an amplifier kit (1/50, TSA Cy3/FITC system; Perkin Elmer, Live Sciences) and slides mounted with Prolong Gold with 4′,6-diamidino-2-phenyl-indole (DAPI).

Inflammation and Gliosis. Macrophages and microglia were visualized using a F4/80 rat Ab (1/100; MCA 497, Biorad)[47] staining. After overnight incubation, donkey anti-rat biotin (1/300; 712-065-153, Jackson) was applied. To investigate gliosis, a mouse Ab against vimentin (1/800; V5255; Sigma-Aldrich Corp.)[48,49] was administered to the 7-μm thick paraffin slices. The following day, the sections were incubated with secondary Ab for 45 minutes (i.e., donkey anti-mouse biotin [1/300, E0433; Dako]). For both stains, the Ab-complex was visualized using the TSA kit and sections were mounted with Prolong Gold with DAPI.

Microscopical Analysis

Neurodegeneration, inflammation, and gliosis were analyzed on images by a masked reader, obtained using a microscope with a digital camera (Axiocam MrC5; Carl Zeiss, Oberkochen, Germany) at a magnification of ×20. Morphometric analyses were performed using commercial software (Metamorph; Leica) on three sections adjacent to both sides of the optic nerve, so in total six sections in the central retina. Analysis was performed 250 μm from the optic nerve head over a length of 250 μm in each section, so in total 12 measurements were averaged. The number of RBPMS-positive cells were counted in the GCL, ChAT-positive cells in the GCL and in the inner nuclear layer (INL) and F4/80-positive cells were counted in all the retinal layers. The number of vimentin-positive fibers crossing the border between the IPL and INL was counted as a measure for gliosis, using a protocol as described by McVicar et al.[47]

Statistics

Prior to statistical analysis, normal distribution of the data was tested using the Shapiro-Wilk test, and equality of variances was determined using the F-test. Measurements between two groups were analyzed using unpaired, two-tailed Student's *t*-test or Mann-Whitney *U* test if data was not distributed normally and/or variances differed significantly. Statistical analysis of inhibitory studies with aflibercept and TAAC were performed with a 1-way ANOVA and longitudinally, time-dependent changes were analyzed with a 2-way repeated measures ANOVA. Data are presented as bars depicting mean + standard error of the mean (SEM), or line graphs showing mean ± SEM. *N* represents the number of animals per condition. All statistical tests were performed using graphing software

TABLE. Body Weight and Glucose Measurements in Diabetic Mice

Treatment Group	Body Weight, g Weeks After STZ Injection			Blood Glucose Level, mg/dL Weeks After STZ Injection		
	−1	8	24	−1	8	24
Nondiabetic	19.6 ± 0.5	28.4 ± 0.6	30.8 ± 0.7	183 ± 6	187 ± 17	180 ± 8
Diabetic	18.9 ± 0.4	21.7 ± 0.5	22.7 ± 0.5	187 ± 10	556 ± 17	477 ± 29

Representative average body weight and blood glucose levels of nondiabetic and diabetic mice. Both treatment groups gained body weight throughout the study ($P < 0.0001$) but the nondiabetic animals were larger compared to diabetic animals at the end of the study ($P < 0.0001$). Blood glucose levels on the other hand were significantly raised in diabetic mice ($P < 0.0001$). Data are shown as mean ± SEM; $n = 5$–12.

(GraphPad Prism version 7.00; GraphPad Software, San Diego, CA, USA). Results were considered significant when $P < 0.05$.

RESULTS

Body Weight and Glucose Measurements in Diabetic Mice

Body weight and blood glucose levels were determined prior to and after STZ injection. Weight increased in all mice until week 24 after diabetes onset. The mice that were buffer-injected showed a higher body weight (30.8 ± 0.7 g) throughout the entire experiment, as compared to STZ-injected mice (22.7 ± 0.5 g) at 24 weeks after diabetes onset.[50] This difference in body weight is consistent with the diabetic phenotype (deterioration of pancreatic β-cell function, coupled to insulin deficiency and systemic hyperglycemia), induced by STZ. STZ-treated mice included in the study, correspondingly showed increased blood glucose levels (477 ± 29 mg/dL) as compared to buffer-injected mice (180 ± 8 mg/dL) up to the end of the study (Table).

These data indicate that five consecutive daily injections of 50 mg/kg of STZ[24] in young mice induced a long-term diabetic phenotype.

Early Decline of Visual Function in Diabetic Mice

To investigate the functional retinal changes in STZ-induced diabetic mice, longitudinal follow-up of the visual response, including visual acuity and CS, was assessed. Diabetic and nondiabetic animals were therefore biweekly subjected to a virtual optomotor test during the entire study period, up to 24 weeks after diabetes onset. Visual function of nondiabetic animals remained unaltered throughout the study, while a significant decline in visual acuity or OKT of 4% ($P < 0.0001$) was already observed during early diabetes (i.e., 4 weeks after diabetes onset), compared to nondiabetic animals. Visual function progressively declined over time, to reach a loss of 14% ($P < 0.0001$) when the study was ended (Fig. 1A). CS was measured at three different spatial frequencies (SF), 0.103, 0.192, and 0.272 cyc/deg, as based on literature.[16] No significant difference was observed between nondiabetic and diabetic animals at the lowest SF (i.e., 0.103 cyc/deg, $P = 0.472$, data not shown). However, diabetic mice showed a reduced CS at a SF of 0.192 ($P < 0.0001$, data not shown) and 0.272 cyc/deg in the late diabetes stage (18 weeks), reaching a decline of 14% ($P < 0.0001$) at 24 weeks, respectively, as compared to control mice (Fig. 1B).

To further evaluate the visual function in the diabetic mice, a subset of diabetic animals received repeated IVT injections with either vehicle or aflibercept (40 μg/eye) at 7 weeks after diabetes onset, after which OKT was measured 1 week posttreatment. Since no differences in CS between nondiabetic and diabetic animals were seen at that time point, CS was not studied after treatment. Vehicle-injected diabetic mice as well as noninjected diabetic animals showed a similar decrease in visual acuity, while aflibercept-injected diabetic animals had a significant decreased visual acuity (3%) compared to vehicle-injected mice (0.354 ± 0.004 vs. 0.366 cyc/deg ± 0.001, respectively, $P < 0.05$; Fig. 1C).

Overall, our findings clearly indicate that STZ-induced DR develops early during disease progression as a speedy decline in visual acuity and eventually also a diminished CS was observed. Repeated injections of a high concentration, compared to a clinically relevant dose, of aflibercept induce an additional, although only small, loss of visual acuity 1 week postdosing.

Early Electroretinogram Changes in Diabetic Mice

To more accurately characterize the decrease of retinal functionality in STZ-injected mice, ERG was applied at 4 and 6 (early), 8 and 12 (mid-), and 20 weeks (late) after diabetes onset.[38] The amplitude of the a- (photoreceptors), b-wave (inner retina), and OPs (amacrine cells) of diabetic mice decreased progressively over the different diabetic stages, whereas a-wave and OP latency (time from stimulus onset to a-wave trough and OP1-3, respectively) and implicit time (time from stimulus to b-wave maximal amplitude following the OPs) progressively increased, as compared to control nondiabetic animals (Figs. 2, 3; time points shown are 6, 12, and 20 weeks after diabetes onset). A detailed graphical overview of overall changes at all time points of a- and b-wave and OPs at different light intensities is provided in Supplementary Figures S1 to S3.

Overall, these ERG data indicate that photoreceptor and inner retinal function are already impaired at early stages during DR development and progressively worsens over time.

Reduced Retinal Thickness Early After Diabetes Onset

Changes in retinal morphology were investigated by using spectral domain optical coherence tomography (SD-OCT) in STZ-injected and control mice at 4 (early), 8 (mid-), and 24 weeks (late) after diabetes onset. Measurements were performed as shown in Figures 4A and 4B. The neural retina was approximately 10 μm (4%, $P < 0.0001$) thinner in diabetic mice, as compared to nondiabetic animals at 8 weeks after diabetes onset and remained thinner until 24 weeks after diabetes onset (Fig. 4C). The GCC complex was thinner at mid- (4 μm or 6%, $P < 0.01$) and late diabetes (2.7 μm or 4%, $P < 0.05$), as compared to control mice (Fig. 4D). Next, NFL-GCL thinning was observed at 4 (9%, 1.3 μm, $P < 0.01$), 8 (12%, 1.6 μm, $P < 0.05$), and 24 (16%, 2.1 μm, $P < 0.01$) weeks after diabetes onset versus nondiabetic animals (Fig. 4E).
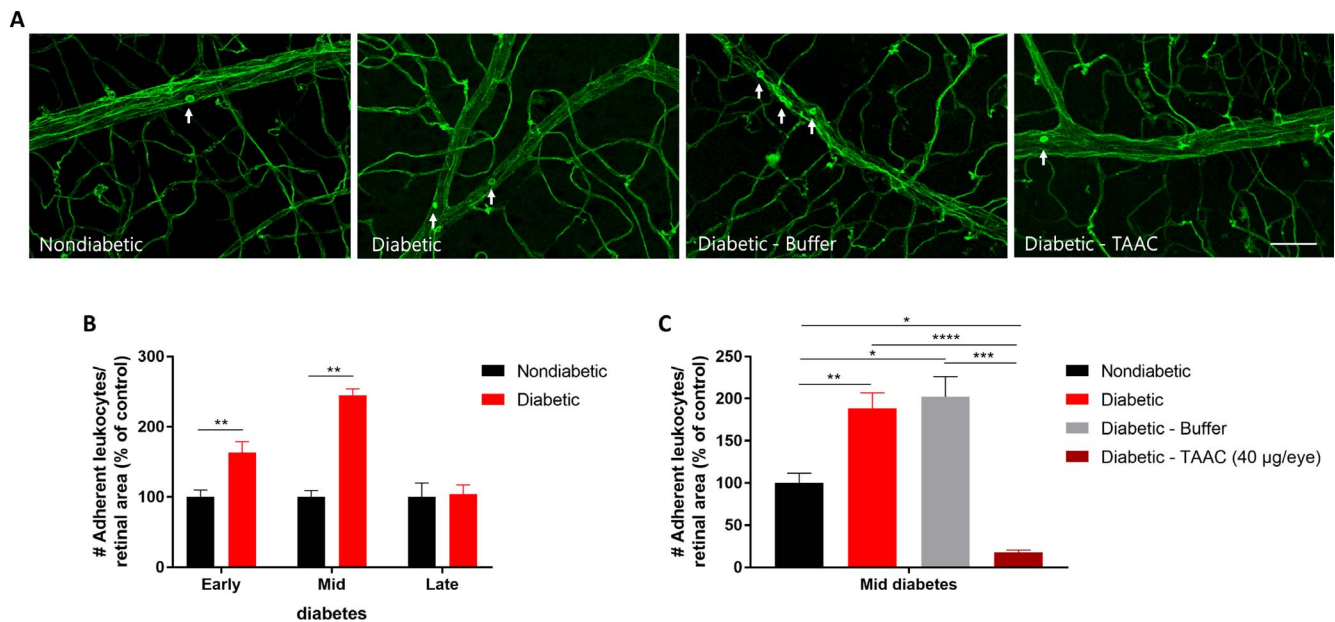
FIGURE 5. Increased number of leukocytes to the retinal blood vessel wall during early- and mid-diabetes. (**A**) Representative pictures of FITC-ConA perfused retinas in nondiabetic (*left panel*), diabetic (*second panel*), diabetic buffer-treated (*third panel*), and diabetic TAAC-treated (*right panel*) mice at 8 weeks after diabetes onset. (**B**) Leukostasis was found to be increased at 2 weeks and peaked at 8 weeks after diabetes onset. (**C**) IVT treatment with TAAC (40 μg/eye), four injections, every other day in week 7 postdiabetes onset, reduced the number of adherent leukocytes with 82% as compared to vehicle-injected animals, evaluated at week 8. Data are shown as mean + SEM, $n = 3–11$, *scale bar*: 50 μm; *white arrows* indicate adherent leukocytes. *$P < 0.05$. **$P < 0.01$. ***$P < 0.001$. ****$P < 0.0001$.

Overall, these results indicate that there is clear, early retinal thinning of the inner retina.

No Detectable Changes in Vascular Leakage in Diabetic Mice

Vascular alterations and leakage are still the main clinical readouts for DR. As such, the mouse STZ model was further characterized by investigating the process of vascular leakage, but no consistent differences between nondiabetic and diabetic animals were detected. First of all, noninvasive FA was biweekly used to longitudinally follow-up leakage from baseline up to 24 weeks postdiabetes onset. The intensity of fluorescein leakage of both the early- or late-phase analysis was not significantly different between the two animal groups at any of the investigated time points (data not shown). At early- and midstage diabetes, vascular leakage was also investigated by means of fluorescent perfusion with FITC-BSA and TRITC-dextran. Fluorescent intensity was determined on retinal whole mounts, but again no differences in vascular leakage between nondiabetic and diabetic mice could be detected upon microscopic analysis (data not shown). Finally, ocular fluorometry (OcuMetrics, Inc.) was used to determine the presence of vitreous leakage in diabetic animals after 8 or 20 weeks postdiabetes onset, but fluorescent levels were not different as compared to those found in nondiabetic animals (data not shown).

Overall, none of the readouts did show any significant or consistent increases in vascular leakage in the diabetic versus control mice, even not during late-term diabetes.

Early Influx of Leukocytes in the Diabetic Retina

Leukostasis is described as one of the earliest events during experimental DR development, which makes it an interesting event to characterize in more detail in the diabetic STZ model.[47,51] Diabetic mice showed a significantly increased number of adherent leukocytes during early- (1.6-fold at 2- and 1.9-fold at 4 weeks postdiabetes; $P < 0.01$, $P < 0.001$) and midterm (2.5-fold increase at 8 weeks postdiabetes; $P < 0.01$) diabetes, versus control animals, and this increased leukocyte adhesion returned to baseline levels at late-stage diabetes (20 weeks postdiabetes; $P = 0.857$; Figs. 5A, 5B). A subset of diabetic animals received repeated IVT injections with either vehicle or triamcinolone acetonide (TAAC, 40 μg/eye), being an anti-inflammatory steroid,[52] at 7 weeks after diabetes onset, and leukostasis was scored 1 week posttreatment. Analysis showed that the inflammatory process was reduced with 82% ($P < 0.001$) in TAAC-injected diabetic mice compared to buffer-injected mice (Figs. 5A, 5C).

These findings suggest that the influx of leukocytes in retinal tissue contributes to an early inflammatory response and that can be counteracted following repeated IVT administrations of a corticosteroid.

Early Inner Retinal Neurodegeneration in the STZ-Induced Diabetic Mouse Model

As inner retinal thinning (SD-OCT) and loss-of-function of inner retinal cells (ERG) was observed in the diabetic mice, further investigation focused on the retinal density of ganglion and cholinergic amacrine cells. RGC density, visualized via RBPMS immunostaining, significantly reduced in the diabetic retina by 17% ($P < 0.05$), 14% ($P < 0.01$), and 20% ($P < 0.05$) during early, mid-, and late diabetes, respectively, as compared to control mice (Figs. 6A, 6B). ChAT immunostaining was performed to stain the cholinergic amacrine cells in the INL and a subset of these cells in the GCL, described as displaced cholinergic amacrine cells. During early diabetes, a nonsignificant decline in the number of ChAT-positive cells in the INL (data not shown; $P = 0.382$), GCL (data not shown; $P = 0.482$) or in both layers was observed ($P = 0.433$; Fig. 6D). However, a significant reduction of 43% and 44% was found during mid-
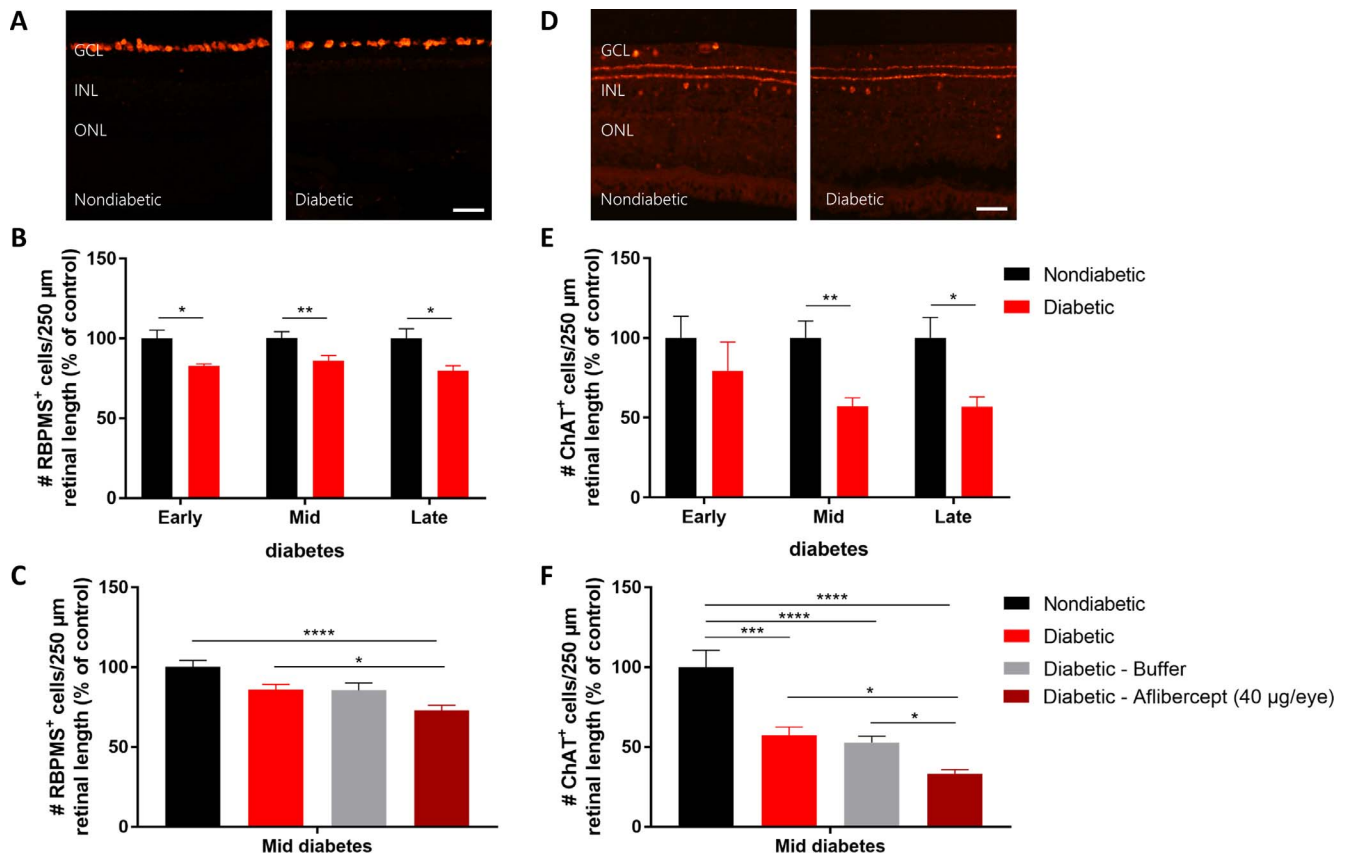
FIGURE 6. Postmortem characterization of neurodegeneration in the STZ-induced diabetic mouse model. (**A**) Representative pictures of RBPMS staining of nondiabetic (*left panel*) and diabetic retinas (*middle panel*) at 8 weeks after diabetes onset. (**B**) Quantitative measurements of RBPMS immunostaining revealed a significant reduction of 17%, 14%, and 20% of viable RGCs, respectively, at 4, 8, and 24 weeks postdiabetes onset. (**C**) Quantification of RBPMS immunopositive cells also disclosed an additional reduced number of viable RGCs (15%) in aflibercept-injected animals compared to buffer-treated mice. (**D**) Cholinergic amacrine cells were stained for ChAT, as shown by representative pictures in nondiabetic (*left panel*) and diabetic mice (*middle panel*) retinas at 8 weeks after diabetes onset, and (**E**) the number of immunopositive cells, counted over a 250 μm retinal length in the GCL and INL, decreased with 43% during mid- and 44% during late-term diabetes. (**F**) The number of cholinergic amacrine cells in diabetic animals was further reduced with 37% when injected with aflibercept (40 μg/eye), as compared to buffer-treated eyes. Data are shown as mean + SEM, $n = 3–11$. *Scale bar*: 50 μm. $*P < 0.05$. $**P < 0.01$. $***P < 0.001$. $****P < 0.0001$.

and at late-term diabetes, as compared to control animals ($P < 0.01$, $P < 0.05$, respectively; Fig. 6E).

To further evaluate if the aflibercept induced decline in visual acuity (OptoMotry) was related to cell type-specific neurodegeneration, the effect of repeated IVT administration of aflibercept (40 μg/eye) on the number of RGCs and cholinergic amacrine cells was investigated at 8 weeks after diabetes onset. Morphometric analysis demonstrated that buffer-injected animals showed a similar level of RGC and cholinergic amacrine cell loss, as compared to noninjected diabetic animals. Remarkably, aflibercept induced an additional reduction of 15% in RGC death, and of 37% for the cholinergic amacrine cells, in contrast to buffer treatment ($P < 0.05$; Figs. 6C, 6F).

Overall, these data indicate that diabetes-induced neurodegeneration already takes place during the early diabetic phase, which eventually evolves in significant loss of inner retinal neurons. Repeated injections of aflibercept induced an additional reduction in the number of RGC and cholinergic amacrine cells at 8 weeks after diabetes onset.

Early Retinal Inflammation and Reactive Gliosis in the STZ-Induced Diabetic Mouse Model

To confirm the early increase of adherent leukocytes in the retinal blood vessels of diabetic mice and to obtain more

information about the role of retinal microglia and invading macrophages during DR progression, a F4/80 staining was performed on retinal sections of the different diabetic phases. A rapid increase of inflammatory cells, mainly observed in the inner retina, was visualized in diabetic animals compared to nondiabetic mice, during early (1.8-fold increase, $P < 0.01$) and mid- (3.1-fold increase, $P < 0.001$) diabetes, which returned to baseline levels at late-stage diabetes (Figs. 7A, 7B). For the investigation of the process of reactive gliosis, a vimentin immunostaining was performed and clearly revealed Müller cell gliosis in eyes of diabetic animals (Fig. 7D). The number of vimentin-positive fibers crossing the IPL/INL border were counted as a measure of gliosis[47] and was found to double during early (1.7-fold increase, $P < 0.05$) diabetes, peaked at midphase diabetes with a 2.7-fold increase ($P < 0.001$), and remained higher in the late diabetic stage (1.9-fold increase, $P = 0.063$, Fig. 7E).

To validate the STZ-induced diabetic mouse model as an appropriate model for the investigation of novel anti-inflammatory drugs, the effect of aflibercept and TAAC (both 40 μg/eye) was studied at 8 weeks after diabetes onset. Repeated IVT injections at week 7, slightly increased inflammation in buffer-injected animals compared to noninjected diabetic mice, which might be procedure-related, as already described in literature.[53] Nonetheless, both aflibercept and TAAC were able
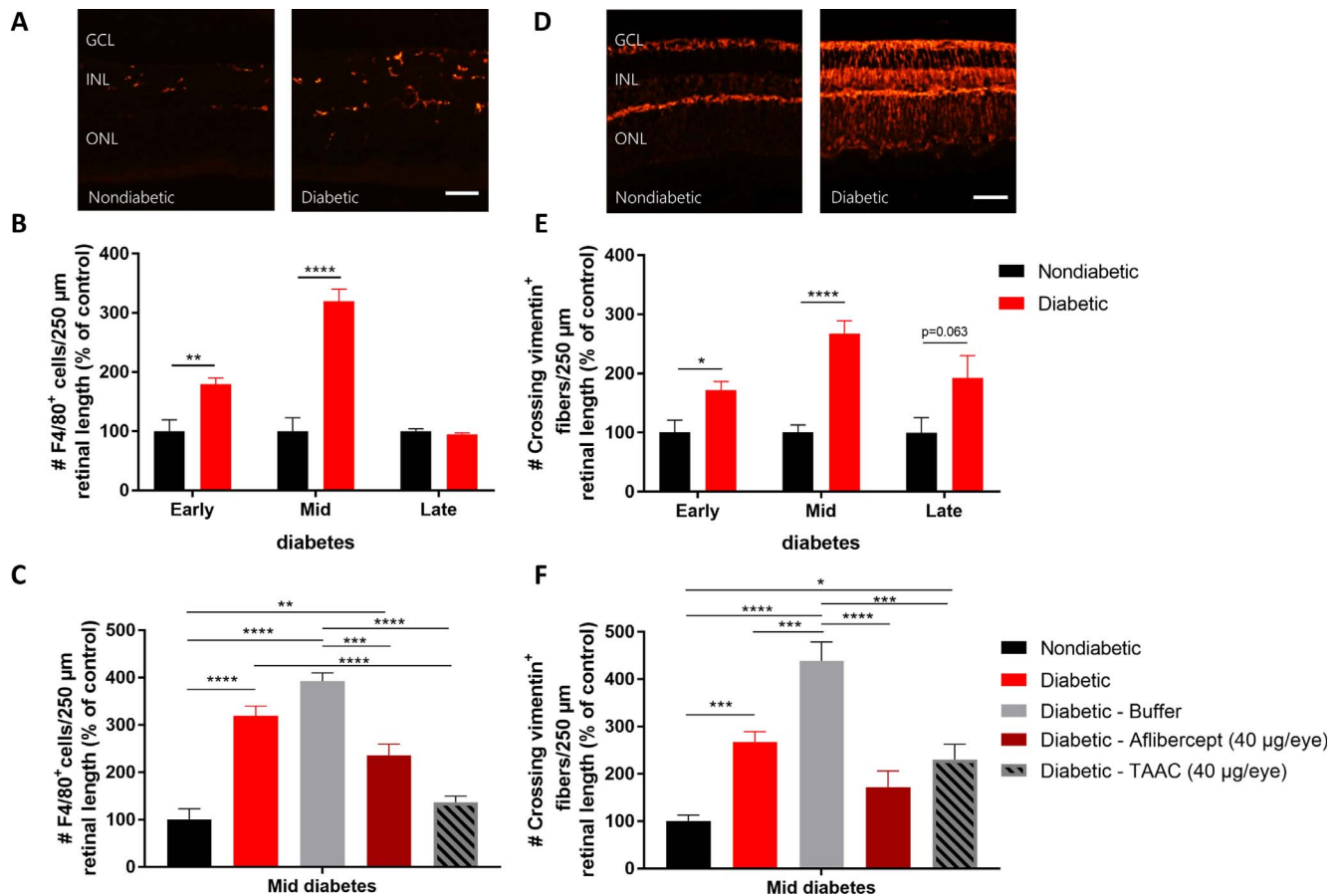
FIGURE 7. Postmortem characterization of inflammation and gliosis in the STZ-induced diabetic mouse model. (A) Representative pictures of F4/80 stained retinas of nondiabetic (left panel) and diabetic mice (middle panel) at 8 weeks after diabetes onset. (B) F4/80 immunostaining showed a rapid increase of inflammatory cells in the early diabetic retina (1.8-fold at 4 weeks), which was more pronounced during midterm diabetes (3.1-fold increase at 8 weeks). When diabetes duration prolonged, the inflammatory response returned back to baseline levels at 24 weeks. (C) Aflibercept and TAAC (both 40 µg/eye) both reduced diabetic-induced influx of inflammatory cells, with 40% and 65%, respectively, compared to buffer-treated animals. (D) Representative pictures of vimentin staining of nondiabetic (left panel) and diabetic retinas (middle panel) at 8 weeks postdiabetes onset. (E) Müller glia reactivity was also studied via histologic staining for vimentin retinal staining and showed significantly more IPL/INL crossing fibers during early (1.7-fold increase) and during midterm diabetes (2.7-fold increase). (F) Gliosis was also diminished with 61% and 48% for aflibercept and TAAC, respectively. Data are shown as mean + SEM, $n = 3$–11. Scale bar: 50 µm. *$P < 0.05$. **$P < 0.01$. ***$P < 0.001$. ****$P < 0.0001$.

to reduce the number of F4/80-positive cells in the retina at 8 weeks after diabetes onset, with a reduction of 40% ($P < 0.001$) and 65% ($P < 0.0001$), respectively (Fig. 7C). These results are in line with those obtained using TAAC for the leukostasis process. Furthermore, aflibercept and TAAC also reduced the number of vimentin-positive fibers, respectively, with 61% ($P < 0.0001$) and 48% ($P < 0.001$), as compared to buffer-injected animals (Fig. 7F).

In conclusion, the mouse STZ model seems to be characterized by an early inflammatory and gliotic response, that respectively returns to baseline or further progresses over time. Administration of two clinically relevant compounds, aflibercept or TAAC, were able to significantly reduce both processes at 8 weeks after diabetes onset.

DISCUSSION

DR is a progressive sight-threatening eye disease, divided in early nonproliferative (NPDR) and late proliferative DR (PDR). Preclinical and clinical studies generally investigate the vascular PDR phase, since it is considered as the most relevant medical pathological hallmark. Moreover, the current standard of care (e.g., anti-VEGF therapy and panretinal photocoagulation) is focused on halting late stage disease progression.[5,54,55] However, more recent studies include research on earlier and preclinical hallmarks of DR, such as inflammation and neurodegeneration. These pathologic processes possibly even precede the vascular phase and might be crucial factors that lie at the onset of the development of sight-threatening PDR and macular edema.[18,19,29] Since partial vision loss might already be evident in undiagnosed DR patients,[16–18] it is essential to further investigate this early stage of the disease, and to eventually integrate the inhibition of these early (initial) processes in novel treatment strategies. Multiple diabetic mouse and rat models are yet available and described (e.g., STZ-induced rodents, Ins2[Akita] mice, Akimba mice, NOD mice, db/db mice, . . .), and most of them are especially studied in the context of retinal vascular leakage. However, none of these models have received an extensive characterization of the early DR phenotype.[24,56–58]

In this study, the mouse STZ model was selected, since this is the most common diabetic mouse model described in literature.[24] Different research groups have used this model to assess vascular leakage,[43,59–62] and although several studies indeed delineated leakage in the diabetic mouse retina, the
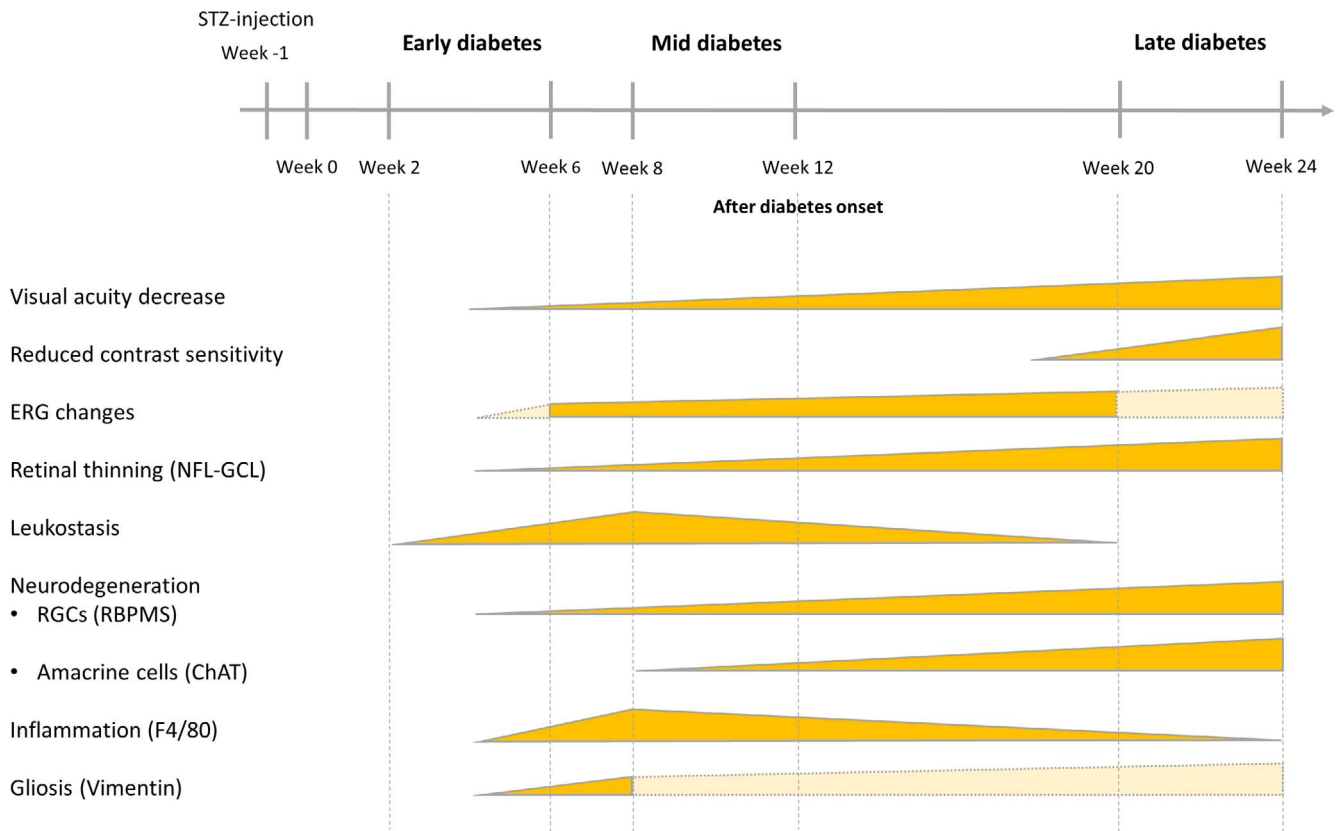
FIGURE 8. Timeline of the significant functional, morphologic and histologic findings observed in the eyes of the STZ-induced diabetic mouse model. The initiation point of the triangles indicates the first observed significant difference in the pathologic process at a specific time point after diabetes onset. Ending of a *triangle* point at a later time point denotes that this pathologic process does not significantly differ any longer between nondiabetic and diabetic animals. *Light yellow* (ERG and gliosis) indicates expected changes based on previously published studies and the observed trend in our own results.

reported findings seem to be difficult to reproduce. Indeed, literature is not conclusive as to the occurrence of leakage in diabetic animal models. Especially the STZ mouse model is mostly described as a model without or with low levels of pathologic vascular changes and leakage. Nevertheless, there have been reports describing the presence of pericyte ghosts after long-term diabetes in STZ mice.[15] Of note, we previously also used this model for the investigation of leakage by means of fluorescent perfusion,[21,63] but encountered a high inter-mouse variability that precludes obtaining reliable results. Although it is recently described that vascular leakage is detectable at 8 weeks via FA,[43] we were not capable to detect it up to 24 weeks after diabetes onset. Ocular fluorometry (Fluorotron; OcuMetrics, Inc., Mountain View, CA, USA) and blood–retinal barrier (BRB) breakdown (Evans blue) are often applied in the STZ rat model and are reliable tools to assess vitreous leakage and BRB breakdown.[64,65] However, our STZ-induced mouse model did not develop vitreous leakage, or the fluorophotometer (OcuMetrics, Inc.) sensitivity was not ideal for the minimal leakage expected in this model, as we could not detect it. Overall, the difficulties to detect retinal/vitreous leakage clearly reveal that vascular leakage is not a prominent hallmark of the STZ-induced diabetic mouse model. Nevertheless, it does present as an adequate model to study the early pathological DR phenotype.[24]

Indeed, using an extensive temporal characterization of the development and progression of diabetic-related cellular responses in the retina, we were able to disclose inflammation, gliosis and neurodegeneration using OptoMotry, ERG, SD-OCT, and immunohistochemical analyses (Fig. 8).

As vision loss in DR patients can eventually lead to complete blindness, the visual response, including visual acuity and CS, was studied as a functional readout in diabetic mice.[66-68] A significantly reduced OKT response was observed from 4 weeks after diabetes onset and onward, indicative of an early loss of visual acuity. Reduced CS only developed at a later time point, thereby confirming previous reports in rodents.[16,32,69] Notably, some other studies reported early CS changes after STZ administration in rodents,[70,71] but these were performed at a spatial frequency of 0.064 cyc/deg, which was not investigated in this study. This, however, cannot explain the difference seen in CS between our study and DR patients in which reduction in CS already develops during early DR.[66] The reason for this difference remains unclear, but indicates that CS might not be an optimal readout for drug testing in the STZ mouse model. Nevertheless, the observed initial loss of visual acuity is a first indication of STZ-induced retinal dysfunction, which is further supported by our ERG results, revealing a significantly increased latency of the OPs and implicit time of the b-wave as well as a reduction of the amplitude at 6 weeks after diabetic onset. Some ERG changes between diabetic and nondiabetic animals were already present at week 4 after diabetes onset, but these were not significantly different (Supplementary Figs. S1–S3). All these results clearly encapsulate the loss of inner retinal function.

Besides these functional retinal assessments, retinal thinning is also regularly studied in DR patients as an indicator for neurodegeneration and vison loss.[42] Morphologic thinning in the NFL-GCL was already described 6 weeks after diabetes onset in STZ-induced mice[29] while another study reported a

reduced total retinal thickness after 10 weeks.[30] These data support our findings, although we observed retinal thinning even earlier, with NFL-GCL and total retinal thinning manifesting at 4 and 8 weeks after diabetes onset respectively, and further declining over time.

In addition, further cell-type specific analysis of diabetes-induced retinal neurodegeneration within the inner retina showed a significant reduction in RGC density starting in the early diabetic phase, further diminishing over time, all in line with earlier findings described in the mouse STZ[21,72,73] and the Ins2[Akita] model.[74] Notably, some contradictory results have been reported in literature, in which neurodegeneration was found to be most prominent in the STZ-induced diabetic mice at later time points (e.g., 10–14 weeks) after diabetes onset,[30] or RGC death was not detected up to 6 months after diabetes induction.[15] Evidently, other inner retinal cell-types, such as cholinergic amacrine cells, can also undergo neurodegeneration. Despite the early delay and reduction of OPs in diabetic patients without clinical DR, these cells remain overlooked in both preclinical and clinical studies.[75] Here we disclosed for the first time loss of cholinergic amacrine cells in the STZ-induced diabetic mouse model, supportive of the observed delay and decrease in OPs during early, mid and late diabetes. Only a few studies describe the loss of cholinergic amacrine cells in other diabetic animal models, being the STZ-induced rat and Ins2[Akita] mouse model. Whereas early loss of dopaminergic amacrine cells was observed in STZ-induced rats,[76] a reduced number of both dopaminergic and cholinergic amacrine was observed in the Ins2[Akita] model, but analysis was only performed after 6 months of diabetes.[46]

The process of early neurodegeneration was further validated in our diabetic mouse model, by demonstrating that both visual acuity, as well as the number of retinal neuronal cells was further decreased after repeated aflibercept administration, as compared to buffer-treated eyes. Aflibercept was selected since it is a clinically relevant compound and VEGF levels are described to be increased in STZ mice.[77,78] The results on reduced RGC density might be surprising, since aflibercept has shown to improve visual acuity in large phase III studies in DME patients (VIVID and VISTA[79,80] and Protocol T[81–83]). However, evidence is being gathered that the use of VEGF inhibitors is associated with deleterious effects on the neuronal cells. Prolonged treatment with anti-VEGF therapy in preclinical models (STZ rat and Ins2[Akita] mice) showed substantial neuronal cell death[84,85] and potential safety concerns are also recently demonstrated in a retrospective study in AMD[86] and DME patients (Filek R, et al. *IOVS* 2017;58:ARVO E-Abstract 2024). Of note, as lower doses did not show any efficacy in the mouse STZ model (data not shown), we used within this preclinical study a high dose of the VEGF-inhibitor (40 µg/eye in a murine eye would represent a high dose of 26 mg/eye in a human condition, compared to the 2 mg of aflibercept that is used in clinical practice). Although we cannot exclude that this high dose of aflibercept might result in an exacerbated neurodegenerative effect after four subsequent IVT injections, our data clearly warrant that care has to be taken upon long-term chronic anti-VEGF treatment.

Neuroinflammation and gliosis are recognized as early key processes in the development of DR,[17,87] which was confirmed by our findings on the increased number of inflammatory cells and vimentin positive Müller cell fibers early after diabetes onset. The observed rapid increase in adherent leukocyte number starting at 2 weeks that still persisted at 4 and 8 weeks after diabetes onset in the murine retina is in line with other STZ studies also indicating a start of leukostasis around 1 to 2 weeks[60,88] and persisting up to 3 months.[51] Although one report describes high leukocyte numbers at 6 months in the mouse STZ model,[89] which contrasts our data that clearly reveal a reduction in the number of adherent leukocytes during late-term diabetes. The reason for this is unknown; however a decline in leukocyte number back to baseline levels is also described in the diabetic Ins2[Akita] model at 20 weeks after diabetes onset.[90]

The rapid retinal influx of leukocytes in hyperglycemic mice, coincides with microglia reactivation as the first responding retinal glial cells, creating an inflammatory environment, most probably provoking the Müller cell gliosis.[23] Microglia reactivity, as leukostasis, initiated early after diabetes onset, peaked during mid-diabetes and diminished later on toward the late diabetes phase. An increased number of retinal microglia has been denoted at 24 weeks after diabetic onset by McVicar et al.,[47] although this augmented number was attributed to resting microglia. Notably, STZ-induction in our model is slightly different from this previous study, where five consecutive daily IP injections were given to mice of 12 weeks of age, which might explain the small shift in time course in the number of microglia returning to baseline levels. On the contrary, Müller cell gliosis seems to be continuously increased during late-stage diabetes, although our results were not significant, possibly due to high biologic variability. In another long-lasting diabetes study, Müller cells were still found to express upregulated GFAP levels after 20 weeks.[91] Importantly, administration of aflibercept[35] or TAAC,[36] were able to significantly reduce both inflammation and macrogliosis at 8 weeks after diabetes onset, which highlight the fact that the mouse STZ model can be used to study novel therapies for DR that halt the inflammatory response. The opposite effect of aflibercept on neurodegeneration and inflammation can be explained by the fact that, although both neuronal and inflammatory cells express VEGF-receptors, both cell types will exert different functions upon ligand binding. Indeed, since VEGF-A is described as important neuroprotective factor,[92] inhibition of this growth factor by aflibercept may have detrimental effects on the neuronal cells. On inflammatory cells, on the other hand, the use of aflibercept will lead to reduced recruitment and migration of inflammatory cells, due to the inhibition of PlGF binding to its receptor.[93]

CONCLUSIONS

Despite the fact that vascular leakage cannot be reliable obtained in the STZ-induced diabetic mouse model, we clearly showed that STZ-induced diabetic mice developed early pathologic hallmarks, from which inflammation seemed to be the initial trigger for further gliosis and neurodegeneration. These then result in the development of functional and morphologic retinal changes, being visual acuity decline, retinal thinning, followed by changes in ERG latencies and amplitudes. Based on these findings, we were able to establish a detailed time line of the nonvascular pathologic processes during DR disease progression (Fig. 8). In addition, it can be concluded that the mouse STZ model can be suitable to target disease hallmarks beyond the vessel pathology and thus to investigate novel integrative therapies to treat DR.

Disclosure: **J. Sergeys**, None; **I. Etienne**, Oxurion (E); **I. Van Hove**, Oxurion (E); **E. Lefevere**, None; **I. Stalmans**, None; **J.H.M. Feyen**, Oxurion (C); **L. Moons**, None; **T. Van Bergen**, Oxurion (E)

References

1. Ogurtsova K, da Rocha Fernandes JD, Huang Y, et al. IDF Diabetes Atlas: global estimates for the prevalence of diabetes for 2015 and 2040. *Diabetes Res Clin Pract*. 2017;128:40–50.

2. You WP, Henneberg M. Type 1 diabetes prevalence increasing globally and regionally: the role of natural selection and life expectancy at birth. *BMJ Open Diabetes Res Care*. 2016;4: e000161.

3. Klein R, Klein BE, Wang Q, Jensen SC. Treatment and control of hypercholesterolemia and hypertension in persons with and without diabetes. *Am J Prev Med*. 1995;11:329–335.

4. Antonetti DA, Klein R, Gardner TW. Diabetic retinopathy. *N Engl J Med*. 2012;366:1227–1239.

5. Stitt AW, Curtis TM, Chen M, et al. The progress in understanding and treatment of diabetic retinopathy. *Prog Retin Eye Res*. 2015;51:156–186.

6. Yau JW, Rogers SL, Kawasaki R, et al. Global prevalence and major risk factors of diabetic retinopathy. *Diabetes Care*. 2012;35:556–564.

7. Gardner TW, Antonetti DA, Barber AJ, LaNoue KF, Levison SW. Diabetic retinopathy: more than meets the eye. *Surv Ophthalmol*. 2002;47(suppl 2):S253–S262.

8. Abcouwer SF. Angiogenic factors and cytokines in diabetic retinopathy. *J Clin Cell Immunol*. 2013 (suppl 1).

9. Hazra S, Konar A. Fibrotic diseases of the eye: potential therapeutic targets. *Eye Diseases and Disorders: A Complete Guide*. Hong Kong: iConcept Press; 2015.

10. Barber AJ. Diabetic retinopathy: recent advances towards understanding neurodegeneration and vision loss. *Sci China Life Sci*. 2015;58:541–549.

11. Adamis AP. Is diabetic retinopathy an inflammatory disease? *Br J Ophthalmol*. 2002;86:363–365.

12. Barber AJ, Baccouche B. Neurodegeneration in diabetic retinopathy: potential for novel therapies. *Vision Res*. 2017; 139:82–92.

13. Joussen AM, Poulaki V, Le ML, et al. A central role for inflammation in the pathogenesis of diabetic retinopathy. *FASEB J*. 2004;18:1450–1452.

14. Tang J, Kern TS. Inflammation in diabetic retinopathy. *Prog Retin Eye Res*. 2011;30:343–358.

15. Feit-Leichman RA, Kinouchi R, Takeda M, et al. Vascular damage in a mouse model of diabetic retinopathy: relation to neuronal and glial changes. *Invest Ophthalmol Vis Sci*. 2005; 46:4281–4287.

16. Alam NM, Mills WCt, Wong AA, Douglas RM, Szeto HH, Prusky GT. A mitochondrial therapeutic reverses visual decline in mouse models of diabetes. *Dis Model Mech*. 2015;8:701–710.

17. Yu Y, Chen H, Su SB. Neuroinflammatory responses in diabetic retinopathy. *J Neuroinflammation*. 2015;12:141.

18. Lynch SK, Abramoff MD. Diabetic retinopathy is a neurodegenerative disorder. *Vision Res*. 2017;139:101–107.

19. Rubsam A, Parikh S, Fort PE. Role of inflammation in diabetic retinopathy. *Int J Mol Sci*. 2019;19:E942.

20. Altmann C, Schmidt MHH. The role of microglia in diabetic retinopathy: inflammation, microvasculature defects and neurodegeneration. *Int J Mol Sci*. 2018;19.

21. Van Bergen T, Hu TT, Etienne I, Reyns GE, Moons L, Feyen JHM. Neutralization of placental growth factor as a novel treatment option in diabetic retinopathy. *Exp Eye Res*. 2017; 165:136–150.

22. Lieth E, Barber AJ, Xu B, et al. Glial reactivity and impaired glutamate metabolism in short-term experimental diabetic retinopathy. Penn State Retina Research Group. *Diabetes*. 1998;47:815–820.

23. Sorrentino FS, Allkabes M, Salsini G, Bonifazzi C, Perri P. The importance of glial cells in the homeostasis of the retinal microenvironment and their pivotal role in the course of diabetic retinopathy. *Life Sci*. 2016;162:54–59.

24. Lai AK, Lo AC. Animal models of diabetic retinopathy: summary and comparison. *J Diabetes Res*. 2013;2013: 106594.

25. Li Q, Verma A, Han PY, et al. Diabetic eNOS-knockout mice develop accelerated retinopathy. *Invest Ophthalmol Vis Sci*. 2010;51:5240–5246.

26. Qian X, Lin L, Zong Y, et al. Shifts in renin-angiotensin system components, angiogenesis, and oxidative stress-related protein expression in the lamina cribrosa region of streptozotocin-induced diabetic mice. *Graefes Arch Clin Exp Ophthalmol*. 2018;256:525–534.

27. Kurihara T, Ozawa Y, Nagai N, et al. Angiotensin II type 1 receptor signaling contributes to synaptophysin degradation and neuronal dysfunction in the diabetic retina. *Diabetes*. 2008;57:2191–2198.

28. Sasaki M, Ozawa Y, Kurihara T, et al. Neurodegenerative influence of oxidative stress in the retina of a murine model of diabetes. *Diabetologia*. 2010;53:971–979.

29. Sohn EH, van Dijk HW, Jiao C, et al. Retinal neurodegeneration may precede microvascular changes characteristic of diabetic retinopathy in diabetes mellitus. *Proc Natl Acad Sci U S A*. 2016;113:E2655–E2664.

30. Martin PM, Roon P, Van Ells TK, Ganapathy V, Smith SB. Death of retinal neurons in streptozotocin-induced diabetic mice. *Invest Ophthalmol Vis Sci*. 2004;45:3330–3336.

31. Saliba A, Du Y, Liu H, et al. Photobiomodulation mitigates diabetes-induced retinopathy by direct and indirect mechanisms: evidence from intervention studies in pigmented mice. *PLoS One* 2015;10:e0139003.

32. Liu H, Tang J, Lee CA, Kern TS. Metanx and early stages of diabetic retinopathy. *Invest Ophthalmol Vis Sci*. 2015;56: 647–653.

33. Tang J, Allen Lee C, Du Y, et al. MyD88-dependent pathways in leukocytes affect the retina in diabetes. *PLoS One*. 2013;8: e68871.

34. Li G, Tang J, Du Y, Lee CA, Kern TS. Beneficial effects of a novel RAGE inhibitor on early diabetic retinopathy and tactile allodynia. *Mol Vis*. 2011;17:3156–3165.

35. Campos Polo R, Rubio Sanchez C, Garcia Guisado DM, Diaz Luque MJ. Aflibercept for clinically significant diabetic macular edema: 12-month results in daily clinical practice. *Clin Ophthalmol*. 2018;12:99–104.

36. Zajac-Pytrus HM, Kaczmarek R, Stronska-Lipowicz D, Pomorska M, Misiuk-Hojlo M. The effects and safety of intravitreal triamcinolone injections in the treatment of diabetic macular edema. *Adv Clin Exp Med*. 2017;26:45–49.

37. Prusky GT, Alam NM, Beekman S, Douglas RM. Rapid quantification of adult and developing mouse spatial vision using a virtual optomotor system. *Invest Ophthalmol Vis Sci*. 2004;45:4611–4616.

38. Huang W, Collette W III, Twamley M, Aguirre SA, Sacaan A. Application of electroretinography (ERG) in early drug

development for assessing retinal toxicity in rats. *Toxicol Appl Pharmacol*. 2015;289:525–533.

39. Kinoshita J, Peachey NS. Noninvasive electroretinographic procedures for the study of the mouse retina. *Curr Protoc Mouse Biol*. 2018;8:1–16.

40. Saul AB, Cui X, Markand S, Smith SB. Detailed electroretinographic findings in rd8 mice. *Doc Ophthalmol*. 2017;134:195–203.

41. van Dijk HW, Kok PH, Garvin M, et al. Selective loss of inner retinal layer thickness in type 1 diabetic patients with minimal diabetic retinopathy. *Invest Ophthalmol Vis Sci*. 2009;50:3404–3409.

42. van Dijk HW, Verbraak FD, Kok PH, et al. Early neurodegeneration in the retina of type 2 diabetic patients. *Invest Ophthalmol Vis Sci*. 2012;53:2715–2719.

43. Chung YR, Choi JA, Koh JY, Yoon YH. Ursodeoxycholic acid attenuates endoplasmic reticulum stress-related retinal pericyte loss in streptozotocin-induced diabetic mice. *J Diabetes Res*. 2017;2017:1763292.

44. Van Hove I, Lefevere E, De Groef L, et al. MMP-3 deficiency alleviates endotoxin-induced acute inflammation in the posterior eye segment. *Int J Mol Sci*. 2016;17:1825.

45. Rodriguez AR, de Sevilla Muller LP, Brecha NC. The RNA binding protein RBPMS is a selective marker of ganglion cells in the mammalian retina. *J Comp Neurol*. 2014;522:1411–1443.

46. Gastinger MJ, Singh RS, Barber AJ. Loss of cholinergic and dopaminergic amacrine cells in streptozotocin-diabetic rat and Ins2Akita-diabetic mouse retinas. *Invest Ophthalmol Vis Sci*. 2006;47:3143–3150.

47. McVicar CM, Ward M, Colhoun LM, et al. Role of the receptor for advanced glycation endproducts (RAGE) in retinal vasodegenerative pathology during diabetes in mice. *Diabetologia*. 2015;58:1129–1137.

48. Li Z, Van Bergen T, Van de Veire S, et al. Inhibition of vascular endothelial growth factor reduces scar formation after glaucoma filtration surgery. *Invest Ophthalmol Vis Sci*. 2009;50:5217–5225.

49. Hippert C, Graca AB, Barber AC, et al. Muller glia activation in response to inherited retinal degeneration is highly varied and disease-specific. *PLoS One*. 2015;10:e0120415.

50. Guo R, Hua Y, Rogers O, Brown TE, Ren J, Nair S. Cathepsin K knockout protects against cardiac dysfunction in diabetic mice. *Sci Rep*. 2017;7:8703.

51. Ishida S, Usui T, Yamashiro K, et al. VEGF164 is proinflammatory in the diabetic retina. *Invest Ophthalmol Vis Sci*. 2003;44:2155–2162.

52. Takata S, Masuda T, Nakamura S, et al. The effect of triamcinolone acetonide on laser-induced choroidal neovascularization in mice using a hypoxia visualization bio-imaging probe. *Sci Rep*. 2015;5:9898.

53. Miyamoto K, Khosrof S, Bursell SE, et al. Vascular endothelial growth factor (VEGF)-induced retinal vascular permeability is mediated by intercellular adhesion molecule-1 (ICAM-1). *Am J Pathol*. 2000;156:1733–1739.

54. Park YG, Roh YJ. New diagnostic and therapeutic approaches for preventing the progression of diabetic retinopathy. *J Diabetes Res*. 2016;2016:1753584.

55. Simo R, Hernandez C. Advances in the medical treatment of diabetic retinopathy. *Diabetes Care*. 2009;32:1556–1562.

56. Robinson R, Barathi VA, Chaurasia SS, Wong TY, Kern TS. Update on animal models of diabetic retinopathy: from molecular approaches to mice and higher mammals. *Dis Model Mech*. 2012;5:444–456.

57. Jiang X, Yang L, Luo Y. Animal models of diabetic retinopathy. *Curr Eye Res*. 2015;40:761–771.

58. Hernandez C, Bogdanov P, Sola-Adell C, et al. Topical administration of DPP-IV inhibitors prevents retinal neurodegeneration in experimental diabetes. *Diabetologia*. 2017;60:2285–2298.

59. Kim SR, Im JE, Jeong JH, et al. The cKit inhibitor, masitinib, prevents diabetes-induced retinal vascular leakage. *Invest Ophthalmol Vis Sci*. 2016;57:1201–1206.

60. He J, Wang H, Liu Y, Li W, Kim D, Huang H. Blockade of vascular endothelial growth factor receptor 1 prevents inflammation and vascular leakage in diabetic retinopathy. *J Ophthalmol*. 2015;2015:605946.

61. Yun JH, Park SW, Kim JH, Park YJ, Cho CH, Kim JH. Angiopoietin 2 induces astrocyte apoptosis via alphavbeta5-integrin signaling in diabetic retinopathy. *Cell Death Dis*. 2016;7:e2101.

62. Lim YC, Bhatt MP, Kwon MH, et al. Prevention of VEGF-mediated microvascular permeability by C-peptide in diabetic mice. *Cardiovasc Res*. 2014;101:155–164.

63. Hollanders K, Van Bergen T, Kindt N, et al. The effect of AMA0428, a novel and potent ROCK inhibitor, in a model of neovascular age-related macular degeneration. *Invest Ophthalmol Vis Sci*. 2015;56:1335–1348.

64. Do carmo A, Ramos P, Reis A, Proenca R, Cunha-vaz JG. Breakdown of the inner and outer blood retinal barrier in streptozotocin-induced diabetes. *Exp Eye Res*. 1998;67:569–575.

65. Canning P, Kenny BA, Prise V, et al. Lipoprotein-associated phospholipase A2 (Lp-PLA2) as a therapeutic target to prevent retinal vasopermeability during diabetes. *Proc Natl Acad Sci U S A*. 2016;113:7213–7218.

66. Stavrou EP, Wood JM. Letter contrast sensitivity changes in early diabetic retinopathy. *Clin Exp Optom*. 2003;86:152–156.

67. Spencer R, McMeel JW, Franks EP. Visual outcome in moderate and severe proliferative diabetic retinopathy. *Arch Ophthalmol*. 1981;99:1551–1554.

68. Gardner TW, Larsen M, Girach A, Zhi X. Protein kinase CDRSSG. Diabetic macular oedema and visual loss: relationship to location, severity and duration. *Acta Ophthalmol* 2009;87:709–713.

69. Aung MH, Kim MK, Olson DE, Thule PM, Pardue MT. Early visual deficits in streptozotocin-induced diabetic long Evans rats. *Invest Ophthalmol Vis Sci*. 2013;54:1370–1377.

70. Aung MH, Park HN, Han MK, et al. Dopamine deficiency contributes to early visual dysfunction in a rodent model of type 1 diabetes. *J Neurosci*. 2014;34:726–736.

71. Allen RS, Hanif AM, Gogniat MA, et al. TrkB signalling pathway mediates the protective effects of exercise in the diabetic rat retina. *Eur J Neurosci*. 2018;47:1254–1265.

72. Yang Y, Mao D, Chen X, et al. Decrease in retinal neuronal cells in streptozotocin-induced diabetic mice. *Mol Vis*. 2012;18:1411–1420.

73. Hollanders K, Hove IV, Sergeys J, et al. AMA0428, a potent rock inhibitor, attenuates early and late experimental diabetic retinopathy. *Curr Eye Res*. 2017;42:260–272.

74. Gastinger MJ, Kunselman AR, Conboy EE, Bronson SK, Barber AJ. Dendrite remodeling and other abnormalities in the retinal ganglion cells of Ins2 Akita diabetic mice. *Invest Ophthalmol Vis Sci*. 2008;49:2635–2642.

75. Lecleire-Collet A, Audo I, Aout M, et al. Evaluation of retinal function and flicker light-induced retinal vascular response in normotensive patients with diabetes without retinopathy. *Invest Ophthalmol Vis Sci*. 2011;52:2861–2867.

76. Ma M, Xu Y, Xiong S, et al. Involvement of ciliary neurotrophic factor in early diabetic retinal neuropathy in streptozotocin-induced diabetic rats. *Eye (Lond)*. 2018;32:1463–1471.

77. Kim YH, Kim YS, Roh GS, Choi WS, Cho GJ. Resveratrol blocks diabetes-induced early vascular lesions and vascular endothelial growth factor induction in mouse retinas. *Acta Ophthalmol*. 2012;90:e31–e37.

78. Li MS, Xin M, Guo CL, Lin GM, Li J, Wu XG. Differential expression of breast cancer-resistance protein, lung resistance protein, and multidrug resistance protein 1 in retinas of streptozotocin-induced diabetic mice. *Int J Ophthalmol*. 2017;10:515–523.

79. Korobelnik JF, Do DV, Schmidt-Erfurth U, et al. Intravitreal aflibercept for diabetic macular edema. *Ophthalmology*. 2014;121:2247–2254.

80. Brown DM, Schmidt-Erfurth U, Do DV, et al. Intravitreal aflibercept for diabetic macular edema: 100-week results from the VISTA and VIVID studies. *Ophthalmology*. 2015;122: 2044–2052.

81. Wells JA, Glassman AR, Ayala AR, et al. Aflibercept, bevacizumab, or ranibizumab for diabetic macular edema. *N Engl J Med*. 2015;372:1193–1203.

82. Wells JA, Glassman AR, Ayala AR, et al. Aflibercept, bevacizumab, or ranibizumab for diabetic macular edema: two-year results from a comparative effectiveness randomized clinical trial. *Ophthalmology*. 2016;123:1351–1359.

83. Cai S, Bressler NM. Aflibercept, bevacizumab or ranibizumab for diabetic macular oedema: recent clinically relevant findings from DRCR.net protocol T. *Curr Opin Ophthalmol*. 2017;28:636–643.

84. Park HY, Kim JH, Park CK. Neuronal cell death in the inner retina and the influence of vascular endothelial growth factor inhibition in a diabetic rat model. *Am J Pathol*. 2014;184: 1752–1762.

85. Hombrebueno JR, Ali IH, Xu H, Chen M. Sustained intraocular VEGF neutralization results in retinal neurodegeneration in the Ins2(Akita) diabetic mouse. *Sci Rep*. 2015;5:18316.

86. Beck M, Munk MR, Ebneter A, Wolf S, Zinkernagel MS. Retinal ganglion cell layer change in patients treated with anti-vascular endothelial growth factor for neovascular age-related macular degeneration. *Am J Ophthalmol*. 2016;167: 10–17.

87. Patel N. Targeting leukostasis for the treatment of early diabetic retinopathy. *Cardiovasc Hematol Disord Drug Targets*. 2009;9:222–229.

88. Leal EC, Manivannan A, Hosoya K, et al. Inducible nitric oxide synthase isoform is a key mediator of leukostasis and blood-retinal barrier breakdown in diabetic retinopathy. *Invest Ophthalmol Vis Sci*. 2007;48:5257–5265.

89. Hossain A, Tauhid L, Davenport I, et al. LRP-1 Pathway targeted inhibition of vascular abnormalities in the retina of diabetic mice. *Curr Eye Res*. 2017;42:640–647.

90. Cardona SM, Mendiola AS, Yang YC, Adkins SL, Torres V, Cardona AE. Disruption of fractalkine signaling leads to microglial activation and neuronal damage in the diabetic retina. *ASN Neuro*. 2015;7.

91. Rungger-Brandle E, Dosso AA, Leuenberger PM. Glial reactivity, an early feature of diabetic retinopathy. *Invest Ophthalmol Vis Sci*. 2000;41:1971–1980.

92. Foxton RH, Finkelstein A, Vijay S, et al. VEGF-A is necessary and sufficient for retinal neuroprotection in models of experimental glaucoma. *Am J Pathol*. 2013;182:1379–1390.

93. Shibuya M. Structure and dual function of vascular endothelial growth factor receptor-1 (Flt-1). *Int J Biochem Cell Biol*. 2001;33:409–420.